Linear Quadratic Regulator based Smooth Transition between Microgrid Operation Modes

Ganjian-Aboukheili, Mohyedin; Shahabi, Majid; Shafiee, Qobad; Guerrero, Josep M.

Published in:
IEEE Transactions on Smart Grid

DOI (link to publication from Publisher):
10.1109/TSG.2021.3094419

Publication date:
2021

Document Version
Accepted author manuscript, peer reviewed version

Linear Quadratic Regulator based Smooth Transition between Microgrid Operation Modes

Mohyedin Ganjian-Aboukheili, Majid Shahabi, *Member, IEEE*, Qobad Shafiee, *Senior Member, IEEE*, and Josep M. Guerrero, *Fellow, IEEE*

***Abstract*—Dual mode operation capability of distributed energy resources in microgrids is an attractive feature that makes these systems a promising solution for improving reliability and economy of the power system. However, the transition between microgrid operation modes (grid-connected and islanding) may lead to a significant deviation in voltage and current because of inconsistency in phase, frequency, and voltage amplitude. To minimize the fluctuations and provide a smooth transition, this paper presents an optimal control framework based on linear quadratic regulator. The framework includes two regulators that separately designed for each transition mode: 1) grid-connected to islanding smooth regulator, and 2) islanding to grid-connected smooth regulator. Optimality based on optimizing solution, smooth transition, ease of implementation due to its simple state feedback form and compatibility with familiar cascade loops are the main advantages of the proposed approach. Experimental results are presented to validate the efficacy of the proposed approach.**

***Index Terms*—Grid-connected, islanding mode, linear quadratic regulator, microgrids, smooth transition.**

NOMENCLATURE

2DOF	2 Degree of freedom	ISGCSR	Islanding to grid-connected smooth regulator
DER	Distributed energy resource	LQR	Linear quadratic regulator
GA	Genetic algorithm	MG	Micro grid
GC	Grid-connected	PCC	Point of common coupling
GCISSR	Grid-connected to islanding smooth regulator	PLL	Phase locked loop
IS	Islanding	SRF	Synchronous reference frame

I. INTRODUCTION

Microgrid (MG) concept has made a revolution in the traditional operation of power system. Indeed, MG is a promising solution for modern power systems where enhancing reliability and resiliency, making economical operation and utilizing small-scale distributed energy resources (DERs) are its brilliant merits. Another distinctive feature of MG is the dual-mode operation capability in grid connected (GC) and islanding (IS) modes [1]. Many of DERs are interfaced via a power electronic converter. The control strategies of DERs depend on MG operation objectives. Two main control strategies of DERs are grid-feeding and grid-forming [2]. Generally, the converter-based DERs operate in grid-feeding strategy in GC mode to inject power without aiming at voltage and frequency regulation. The grid-forming strategy is usually related to IS mode where the main control objectives of DERs are voltage and frequency regulation over the MG and proper power sharing. However, in order to decrease the intermittency of renewable energy resources, they may be operated under grid-feeding strategy in both modes of operation. Various control strategies have been introduced for both operation modes of MGs in the literature [3], [4].

One of the characteristics of reliability enhancement of modern power systems using MGs is their ability to supply demands in the islanding mode as well as seamless transition from GC to IS mode when MG disconnects from the main grid intentionally or unintentionally [5]. Once the circuit breaker is opened at point of common coupling (PCC), there is a short period with no voltage control source e.g. main grid or DER with grid-forming strategy, which may makes large disturbances and endanger the MG operation. Generally, during transition, significant fluctuation may appear in the MG variables, which can disrupt safe operation of the system. Moreover, this situation may happen in the resynchronizing process where MG is reconnected to the grid. Therefore, a seamless transfer with a smooth response is a worthy requirement. The performance of the DER controllers directly shapes the DER output response during a disturbance. Indeed, if this phenomenon is not managed competently, the MG may suffer fatal transients or even stability threats. Thus, one of the objectives of the DER controller must be disturbance elimination or at least efficient disturbance mitigation.

Different control techniques have already been proposed to have a good performance in both modes of operation. Some of the proposed control strategies based on advanced control theory are sliding-mode [6], adaptive back stepping [7], and model predictive control [8], [9]. Although these algorithms provide a single scheme in both modes of operation, they have a complex structure and are not easily implemented.

The authors acknowledged the funding support of Babol Noshirvani University of Technology through grant program no. BNUT/370445/99.

M. Ganjian-Aboukheili and M. Shahabi are with Department of Electrical and Computer Engineering, Babol Noshirvani University of Technology, Babol, Iran (e-mail: m.ganjian@stu.nit.ac.ir; shahabi.m@nit.ac.ir). Q. Shafiee is with the Department of Electrical Engineering, University of Kurdistan, Sanandaj, Kurdistan, Iran (e-mail: q.shafiee@uok.ac.ir). J. M. Guerrero is with the Institute of Energy Technology, Aalborg University, Aalborg, Denmark (e-mail: joz@et.aau.dk).

Alternatively, majority of the presented control schemes in the literature are based on classical linear control theory. A single control scheme based on voltage controller is introduced in [10] where voltage and frequency references are provided by droop control. To cope with poor dynamic behavior of the droop mechanism, modified droop control is presented in [11] while disturbance rejection remains unaddressed. A control strategy based on disturbance observer is introduced in [12] to overcome the above mentioned problem where the uncertainty of the parameters is also studied. However, this control strategy is used for different schemes in GC and IS modes where the large transients in voltage and current may appear at switching time. The strategy also neglects the transition time.

Cascade control strategies based on voltage-current loops have already been proposed in the literature (e.g., [13-20] which are based on two different schemes; grid-feeding strategy in GC mode and grid-forming strategy in IS mode). Although simple structure, easy implementation, and good performance are the advantages of this technique, output fluctuations of DERs may be intensified due to controller transferring during MG transition. During transition, transient signals caused by hard switching. If the controller realization and initialization strategies are poorly designed for switching, substantial transient signals caused by the switching can degrade the performance and lead to instability. To address this challenge, authors in [13] present a control framework composed of proportional-resonance controller and the feedback linearization technique. Reference [14] proposed a general control scheme for the operation of a MG where a diesel generator-set is utilized to support MG in the worst condition. It is clear that the diesel generator could improve transition disturbances because of enough inertia. In [17] an indirect current control with two cascade loops of capacitor voltage loop and grid current loop is presented to ensure seamless transfer between the operation modes. A linear quadratic regulator (LQR)-based control strategy is developed in [18] for a multiple mode switched control. Bumpless transfer of MG is provided by two separate compensators. However, dynamic of the phase locked loop (PLL) in GC mode and the voltage control loop in IS mode are unaddressed during transition. To have a better disturbance rejection for a multiple mode control, robust control techniques are used in [19] and [20]. A set of kalman filters are used to estimate output signals. The performance of the approach is dependent on kalman filters design. These technique has a very complex design procedure and difficult to be implemented because of their nonlinear time-variant nature. A modified voltage controller with an adaptive droop based power controller is proposed in [21] to facilitate only the smooth islanding transition. In [22], authors propose a new adaptive control structure based on internal model control. Although the proposed controller is validated by experimental results, the model must be exactly matched with the plant to have accurate design and performance. Several efforts have been also executed using data transfer between DERs and PCC for seamless transfer [23], [24]. Seamless transfer of MGs is studied in [25], and [26] using distributed control approach. However, MGs operation may be worsened due to any failure in communication links.

To abstain from the complexity of nonlinear techniques and communication-based strategies, linear strategy with improved dynamic performance is the focus of this paper. An optimal control technique based on LQR is proposed to bring a smooth transition for MGs when switching between the operations modes. Motivated by the aforementioned principles, the main contributions of this paper are as follows.

- Unlike the work in [18] which only uses a droop control in grid-forming strategy while the inner loops are neglected, the proposed method includes the dynamic model of inner control loops in grid-forming strategy and provides a control design procedure.
- Opposed to the work in [18], PLL dynamic is also developed in the grid-feeding strategy during reconnection transition.
- The potential effects of imperfect islanding detection algorithm and premature reconnection process are analyzed to show robustness of the proposed strategy.
- For the better clarification, the proposed control strategy is also validated by experimental results.

In following, section II describes the basis of the smooth linear quadratic regulator and its design procedure. Application of LQR on dual-mode control strategy of a converter-based DER is evaluated in section III. Experimental results are described in section IV. Section V presents the conclusion.

II. Proposed 2 degree of freedom (2DOF) Smooth LQR

The fundamental of a smooth LQR controller is expressed in this section. Let us consider a plant with two different control strategies as shown in Fig. 1. In such a strategy, at any time the system is governed by one controller called online controller and the other one called off-line controller will be standby until transfer command is issued and the system switches to off-line controller. Both controllers have their specific inputs including set-point $r_{1,2}$ and feedback of measurement signal $y_{1,2}$. Here, 2 DOF configuration means that both of the controllers are driven by the set-points and feedback of the system outputs. Due to different set-points and error signals that are fed to online and off-line controllers, large transients may happen at the transferring time in the output of the system. As a solution, in order to mitigate the transients, both controllers must generate similar outputs [27]. A seamless transfer between different controllers can be realized by the LQR scheme and state-feedback theory with an objective function that minimizes such transferring transients.

A. Smooth regulator fundamental

According to Fig. 1, the system is supposed to operate under the controller which is called online controller with set-point r_2; however, the off-line controller driven by r_1, is not applied to the system. There are two control switches including the system input switch and the off-line controller input switch.

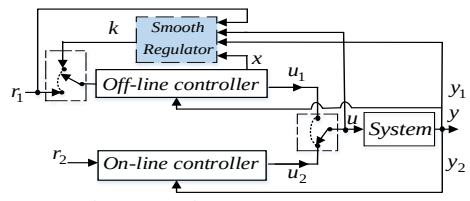

Fig. 1. 2DOF configuration of the smooth linear quadratic regulator.

This article has been accepted for publication in a future issue of this journal, but has not been fully edited. Content may change prior to final publication. Citation information: DOI 10.1109/TSG.2021.3094419, IEEE Transactions on Smart Grid

The off-line controller is derived by k and set-point r_1 before and after the switching time, respectively. To ensure a smooth transition, it is necessary that the off-line controller follow the online controller properly. Therefore, two main goals for LQR objective function can be defined as:

$$E_u(t) = u_1(t) - u_2(t) \ , \ E_e(t) = k(t) - r_1(t) \tag{1}$$

where $E_u(t)$ and $E_e(t)$ are the controllers' output error and the error of the off-line controller input, respectively.

An objective function for the LQR can be stated as [27]:

$$J(u_2, k) = \frac{1}{2}\int_0^T E_u^T(t) W_u E_u(t) + E_e^T(t) W_e E_e(t) dt \tag{2}$$

where W_u and W_e are positive definite matrices to determine the weighting of $E_u(t)$ and $E_e(t)$. To solve the objective function, it is necessary to extract state space model of the off-line controller. State space model of a 2DOF system configuration, regarding off-line controller, can be described as:

$$\dot{x} = Ax + B_1 k + B_2 y_1 \ , \ u_1 = Cx + D_1 k + D_2 y_1 \tag{3}$$

By substituting (3) in (1) and then in (2), the objective function is formed as:

$$\begin{aligned} J = \frac{1}{2}\int_0^{T_0} [(Cx + D_1 k + D_2 y_1 - u_2(t))^T W_u (Cx + D_1 k + D_2 y_1 - u_2(t)) \\ + (k(t) - r_1(t))^T W_e (k(t) - r_1(t))] \, dt \end{aligned} \tag{4}$$

The equality constraints of (3) can be joined to the objective function (4) by Lagrange multiplier, $\lambda(t) \in R^n$. Thus, (4) is rewritten as:

$$\mathcal{J} = \int_0^{T_0} [H(t) - \lambda(t)^T \dot{x}(t)] dt \tag{5}$$

where the Hamiltonian, $H(t)$, is expressed as follows:

$$\begin{aligned} H(t) = \frac{1}{2}\Big[[(Cx + D_1 k + D_2 y_1 - u_2(t))^T W_u (Cx + D_1 k + D_2 y_1 - u_2(t)) \\ + (k(t) - r_1(t))^T W_e (k(t) - r_1(t)) + \lambda^T (Ax + B_1 k + B_2 y_1)] \end{aligned} \tag{6}$$

First order necessary conditions for the optimality of (5) are provided as follows:

$$\dot{x} = \frac{\partial H}{\partial \lambda} \ , \ \dot{\lambda} = -\frac{\partial H}{\partial x} \ , \ 0 = \frac{\partial H}{\partial k} \tag{7}$$

Using the proposed lemma in [27], the optimal solution of the objective function (4) is obtained as follows:

$$\begin{aligned} k = -(D_1^T W_u D_1 + W_e)^{-1} [(D_1^T W_u C)^T x + B_1 \lambda \\ + (D_1^T W_u D_2)^T y_1 - D_1^T W_u u_2 - W_e r_1] \end{aligned} \tag{8}$$

Eq. (8) can be written as a state feedback matrix multiplied by a vector. The vector includes the state variables of the off-line controller, Lagrange multiplier, system outputs, outputs of the online controller, and off-line set point as follows.

$$k = -(D_1^T W_u D_1 + W_e)^{-1} \begin{bmatrix} (D_1^T W_u C)^T \\ B_1 \\ (D_1^T W_u D_2)^T \\ -D_1^T W_u \\ -W_e \end{bmatrix}^T \begin{bmatrix} x \\ \lambda \\ y_1 \\ u_2 \\ r_1 \end{bmatrix} \tag{9}$$

The Lagrange multiplier λ is determined as:

$$\lambda = Px - g \tag{10}$$

where P is the solution of a Differential Riccati Equation (DRE). With assuming an infinite time horizon for DRE, the solution has a time-invariant value and it can be rendered to Algebraic Riccati Equation (ARE) as follows:

$$0 = P\hat{A} + \hat{A}P + P\hat{B}P + \hat{C} \tag{11}$$

where

$$\hat{A} = A + B_1[(-D_1^T W_u D_1 + W_e)^{-1}] D_1^T W_u C \tag{12}$$

$$\hat{B} = B_1[(-D_1^T W_u D_1 + W_e)^{-1}] B_1^T \tag{13}$$

$$\hat{C} = C^T W_u [I + W_u D_1 [(-D_1^T W_u D_1 + W_e)^{-1}] D_1^T W_u] C \tag{14}$$

The necessary and sufficient conditions of the existence a stable solution for (11) are controllability of ($\hat{A}$, $\hat{B}$) and observability of ($\hat{A}$, $\sqrt{\hat{C}}$). The g in (10) is described as follow:

$$\dot{g} = -\left(\hat{A}^T + P\hat{B}\right) g - B_g \hat{\omega} \tag{15}$$

where

$$B_g = \begin{bmatrix} -(C^T W_u D_1 \Delta D_1^T W_u D_2 + C^T W_u D_2 + P(B_2 + B_1 \Delta D_1^T W_u D_2))^T \\ (C^T W_u D_1 \Delta D_1^T W_u + C^T W_u + P B_1 \Delta D_1^T W_u)^T \\ (C^T W_u D_1 \Delta W_e + P B_1 \Delta W_e)^T \end{bmatrix}^T \tag{16}$$

and $\hat{\omega} = [y_1, u_2, r_1]^T$ is an exogenous vector.

According to optimal control theory, the differential equation (15) does not converge to a constant solution for an arbitrary exogenous vector. Using the proposed lemma in [27], an approximation for g can be considered as:

$$g = -\left(\hat{A}^T + P\hat{B}\right)^{-1} B_g \hat{\omega} \tag{17}$$

By solving (11) and calculating g in (17), λ in (10) can be obtained. By replacing λ in (9), the final form of solution k for infinite time horizon can be determined as:

$$k = \underbrace{(D_1^T W_u D_1 + W_e)^{-1} \begin{bmatrix} (D_1^T W_u C + B_1^T P)^T \\ (D_1^T W_u D_2 - B_1^T M \hat{Y})^T \\ (-D_1^T W_u + B_1^T M \hat{U})^T \\ (-W_e + B_1^T M \hat{R})^T \end{bmatrix}^T}_{SF} \begin{bmatrix} x \\ y_1 \\ u_2 \\ r_1 \end{bmatrix} \tag{18}$$

where

$$M = \left(\hat{A}^T + P\hat{B}\right)^{-1} \tag{19}$$

$$\begin{aligned} \hat{Y} = (C^T W_u D_1 + P B_1)[-(D_1^T W_u D_1 + W_e)^{-1}] D_1^T W_u D_2 \\ + P B_2 + C^T W_u D_2 \end{aligned} \tag{20}$$

$$\hat{U} = C^T W_u + (C^T W_u D_1 + P B_1)[-(D_1^T W_u D_1 + W_e)^{-1}] D_1^T W_u \tag{21}$$

$$\hat{R} = (C^T W_u D_1 + P B_1)[-(D_1^T W_u D_1 + W_e)^{-1}] W_e \tag{22}$$

According to (18), it can be concluded that the state feedback matrix *SF* is a time-invariant matrix, with easy calculation and implementation.

B. Smooth regulator design procedure

In order to apply the proposed approach to any system, a systematic procedure of calculating state feedback matrix *SF* is expressed in Fig. 2. At first, the state space of the off-line controller should be derived. To have a stable and smooth response during transition, the dominant eigenvalues of the closed-loop of the off-line controller are determined in such a way that its output (u_1) tracks the online controller output (u_2) with a minimum error. The linear control design criteria such as settling time, overshoot percentage, and rise time could be used to specify the desired eigenvalues of the off-line controller.

This article has been accepted for publication in a future issue of this journal, but has not been fully edited. Content may change prior to final publication. Citation information: DOI 10.1109/TSG.2021.3094419, IEEE Transactions on Smart Grid

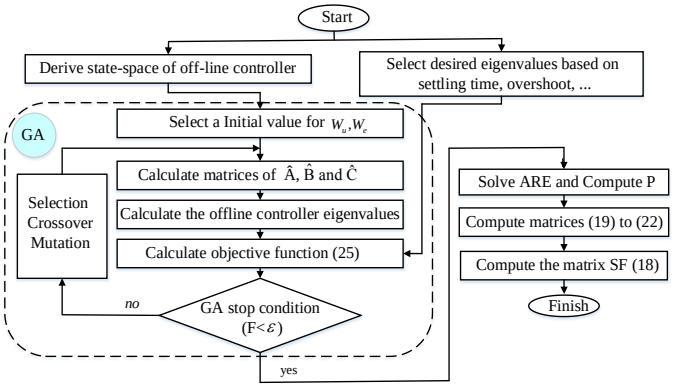

Fig. 2. Systematic procedure of calculating the state feedback matrix of the proposed smooth regulator.

The general form of the closed-loop system of the off-line controller are expressed in (23) and (24).

$$A_{closed\ loop} = A - B_1 k_1 \tag{23}$$

$$k_1 = -(D_1^T W_u D_1 + W_e)^{-1}(B_1^T P + D_1^T W_u C) \tag{24}$$

According to (23) and (24), matrices W_e and W_u play an important role in the system transient response. W_e and W_u matrices can be determined using pole placement technique based on an evolutionary algorithm such as genetic algorithm (GA) aiming at desirable system response. Indeed, the W_e and W_u matrices are determined in such a way that the errors between the closed-loop poles location of the off-line controller and the desired poles location are converged to a very small value. This solution could be expressed as follows:

$$Min\ \ Obj.\ F = \sum_i \left(\left|\lambda_i^{des}\right| - \left|\lambda_i^{off}\right| \right)^2 (1 + Pen \times N) \tag{25}$$

where λ_i^{des} is the desired eigenvalues and λ_i^{off} is the off-line controller eigenvalues. To guarantee the controllability and observability conditions, a penalty (*Pen*) is defined as follows:

$$Pen = pen_{ctrb} + pen_{obsv} \tag{26}$$

$$pen_{ctrb} = \begin{cases} 0 & \text{if } (\hat{A}, \hat{B}) \text{ is } controllable \\ 1 & \text{if } (\hat{A}, \hat{B}) \text{ is not } controllable \end{cases} \tag{27}$$

$$pen_{obsv} = \begin{cases} 0 & \text{if } (\hat{A}, \sqrt{\hat{C}}) \text{ is } observable \\ 1 & \text{if } (\hat{A}, \sqrt{\hat{C}}) \text{ is not } observable \end{cases} \tag{28}$$

N is a large enough positive constant. Elements of W_e and W_u matrices are GA decision variables.

III. Application of LQR on Microgrids

In this section, implementation of the proposed approach on an inverter-based DER with both modes of operation (GC and IS) are studied. Fig. 3 shows the physical part of the inverter with its control scheme. Control strategies in GC and IS modes are grid-feeding and grid-forming, respectively. A control switch is used to change the control strategies upon receiving a triggered signal. The DER is connected to its local bus thanks to a LCL filter. Without losing the generality, the dynamic of prime mover side of the DER is neglected and modeled by a DC source. Since smooth transition between operation modes of MG is the focus of the paper, two smooth regulators are used to guarantee our objective in two transition modes; a) GC to IS and b) IS to GC.

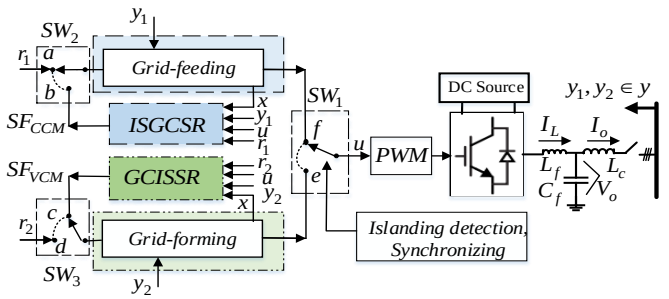

Fig. 3. Physical and control scheme of an inverter based DER connected to the MG.

A. GC to IS Smooth Regulator Design Procedure

Let us consider the DER is working under grid-feeding strategy in GC mode. An unintentional islanding event will occur consequent to a disturbance in the main grid. Thus, MG goes to the islanding mode where regulating the voltage and frequency with smooth transition and proper power sharing are the desired objectives.

To design the GC to IS Smooth Regulator (GCISSR), the grid-forming strategy is considered as an off-line controller which is governed by state feedback matrix SF_{VCM}. This control strategy becomes online in islanding mode with set-points $r_2 = [P^*, Q^*, \omega^*, E_d^*, E_q^*]$. $u_2 = [\theta_2, V_{d2}, V_{q2}]$ is the output vector of the control strategy. Hence, the state space model of grid-forming strategy must be derived. The cascade loops approach is an attractive solution to control an inverter [28]. Fig. 4(a) shows the block diagram of the DER with three control loops including power, voltage and current loops. The power controller is based on droop control that generates references for the voltage loops. The simplified block diagram of the off-line controller is depicted in Fig. 4(b) where state variables are also defined. The droop mechanism is composed of *P-f* and *Q-V* characteristics. To derive the state space model of the off-line controller, the droop equation can be rewritten as follows:

$$\omega = \omega^* - m(p_o - P^*)\frac{w_c}{s + w_c} \tag{29}$$

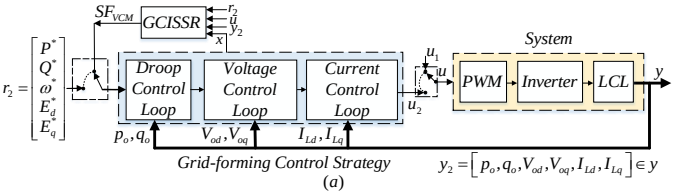

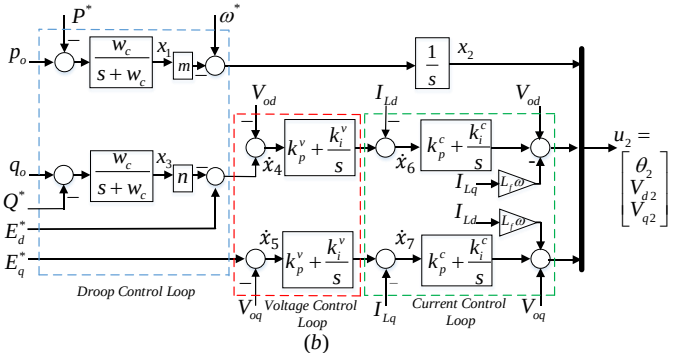

Fig. 4. Grid-forming overall structure of a DER: (a) schematic of off-line control governed by smooth regulator, (b) control block diagram with state variables definition.

This article has been accepted for publication in a future issue of this journal, but has not been fully edited. Content may change prior to final publication. Citation information: DOI 10.1109/TSG.2021.3094419, IEEE Transactions on Smart Grid

$$E_d = E_d^* - n(q_o - Q^*)\frac{w_c}{s+w_c}, \quad E_q = E_q^* = 0 \tag{30}$$

where, ω is the inverter angular frequency. E_d and E_q are direct and quadrant sequence of inverter output voltage. Ouput active and reactive power of inverter are p_o and q_o, and P^* and Q^* are their references. ω^*, E_d^*, and E_q^* are references of angular frequency, direct and quadrant voltage of droop mechanism, respectively. A low pass filter with cut-off frequency w_c is used to reject high frequency components during power measurement [21]. According to Fig. 4(b) and (29), (30), the state space model of the off-line controller can be obtained as:

$$\dot{x}_1 = -x_1 w_c + w_c(p_o - P^*), \quad \dot{x}_2 = \omega^* - m x_1 \tag{31}$$

$$\dot{x}_3 = -x_3 w_c + w_c(q_o - Q^*), \quad \dot{x}_4 = E_d^* - n x_3 - V_{od} \tag{32}$$

$$\dot{x}_5 = E_q^* - V_{oq} \tag{33}$$

$$\dot{x}_6 = k_i^v x_4 - k_p^v n x_3 + k_p^v E_d^* - k_p^v V_{od} - I_{Ld} \tag{34}$$

$$\dot{x}_7 = k_i^v x_5 + k_p^v E_q^* - k_p^v V_{oq} - I_{Lq} \tag{35}$$

The output equations of the grid-forming control strategy are defined as:

$$\theta_2 = x_2 \tag{36}$$

$$V_{d2} = k_i^c x_6 + k_i^v k_p^c x_4 - k_p^v k_p^c n x_3 + k_p^v k_p^c E_d^* + (1 - k_p^v k_p^c) V_{od} - k_p^c I_{Ld} - L_f w_0 I_{Lq} \tag{37}$$

$$V_{q2} = k_i^c x_7 + k_i^v k_p^c x_5 + k_p^v k_p^c E_q^* + (1 - k_p^v k_p^c) V_{oq} - k_p^c I_{Lq} + L_f w_0 I_{Ld} \tag{38}$$

Using (31) to (38), coefficient matrices of (3) for the grid-forming strategy are obtained (see Appendix A). According to Fig. 2, the matrix SF_{VCM} is calculated and presented in Appendix C.

B. IS to GC Smooth Regulator Design Procedure

The general structure of the grid-feeding strategy of a DER is shown in Fig. 5. The controller is implemented in synchronous reference frame (*SRF*). The control strategy is off-line in IS mode and governed by state feedback matrix SF_{CCM}. This matrix is provided by IS to GC Smooth Regulator (ISGCSR). While, in GC mode $r_1 = [V_q^*, \omega^*, I_{Ld}^*, I_{Lq}^*]$ is set-point vector of the control strategy. In addition, $u_1 = [\theta_1, V_{d1}, V_{q1}]$ is output vector of the grid-feeding control strategy. The *dq* values of variables can be obtained using the park's transform with a PLL to extract the phase of voltage. The performance of DER with grid-feeding strategy directly depends on the PLL behavior (e.g. especially during transition). So, the PLL dynamics are considered through integrating into the SRF-current control loop as shown in Fig. 5(b). The MG can be reconnected to the main grid at PCC when it is available. Thus, it is necessary that the voltage of both sides of PCC must be synchronized. The synchronization criteria can be found in IEEE.std.1547 which are ±10% voltage magnitude, 0.3 Hz and 20 degree [29]. When the standard criteria is satisfied, the closing signal is triggered and sent to the PCC circuit breaker. In [28], a straightforward solution is proposed where phase and amplitude difference signals are provided by both side voltage of PCC in the stationary reference frame.

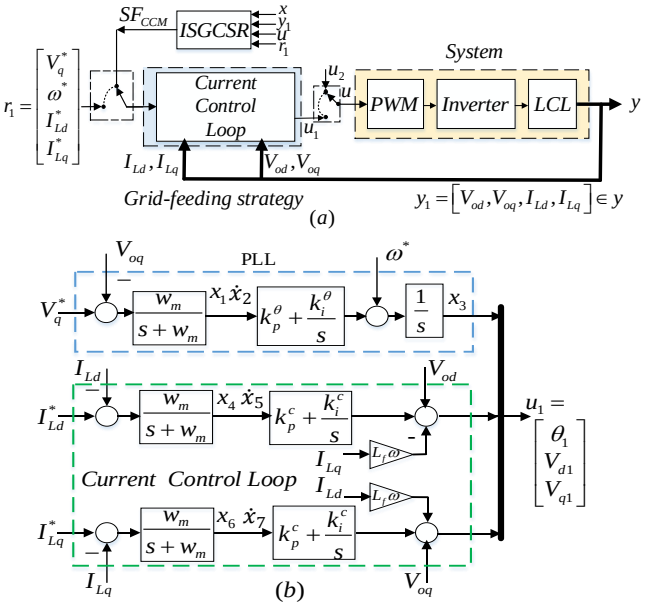

Fig. 5. Grid-feeding overall control strategy of a DER: (a) schematic of off-line control governed by smooth regulator, (b) control block diagram with state variables definition.

The mismatches of the angular frequency and voltage amplitude are added to droop control to adjust MG side voltage. Moreover, to guarantee a smooth transition from islanding mode to GC mode, ISGCSR is developed to bring grid-feeding strategy into online smoothly. To design the ISGCSR, the state space model of the grid-feeding strategy required to be obtained. State variables x_1, x_2 and x_3 represent the dynamics of PLL. A measurement low pass filter with cut-off frequency w_m is used. Using this modification in the conventional SRF-current control loop, state space model will be controllable and observable. The rest of state variables represent the dynamic of SRF-current controller (see Fig. 5(b)). The state space model of the grid-feeding strategy is obtained by following equations:

$$\dot{x}_1 = -x_1 w_m + w_m(V_q^* - V_{oq}), \quad \dot{x}_2 = x_1 \tag{39}$$

$$\dot{x}_3 = \omega^* + k_p^\theta x_1 + k_i^\theta x_2, \quad \dot{x}_4 = -x_4 w_m + w_m(I_{Ld}^* - I_{Ld}) \tag{40}$$

$$\dot{x}_5 = x_4, \quad \dot{x}_6 = -x_6 w_m + w_m(I_{Lq}^* - I_{Lq}) \tag{40}$$

$$\dot{x}_7 = x_6 \tag{41}$$

and the outputs are:

$$\theta_1 = x_3 \tag{42}$$

$$V_{d1} = k_i^c x_5 + k_p^c x_4 + V_{od} - L_f w_0 I_{Lq} \tag{43}$$

$$V_{q1} = k_i^c x_7 + k_p^c x_6 + V_{oq} + L_f w_0 I_{Ld} \tag{44}$$

The coefficient matrices of (3) for grid-feeding strategy are presented in Appendix B and the output of ISGCSR, SF_{CCM} is presented in Appendix C. To ensure a smooth transition, the off-line controller should follow the online controller properly. This behavior is affected by W_u and W_e matrices. It is clear that poles of the off-line controller are manipulated toward desired locations using the proposed state feedback matrix. W_u and W_e can be obtained using dominant poles placement technique. The dominant poles of the off-line controller are specified using a settling time of 100*ms* and damping ratio of 0.707.

This article has been accepted for publication in a future issue of this journal, but has not been fully edited. Content may change prior to final publication. Citation information: DOI 10.1109/TSG.2021.3094419, IEEE Transactions on Smart Grid

IV. Simulation Results

To verify the effectiveness of the proposed approach, the microgrid, as depicted in Fig. 6, has been used. For this study, all 4 DERs are inverter-based sources with the same capacity of 30 kW. They have been equipped with two sets of controllers for dual mode operations. Two smooth regulators are designed and applied on each DER to facilitate a smooth transition between the MG operation modes. The MG is simulated in the MATLAB/Simulink environment. The simulation and test case data are given in Table I. To show the effects of inner loop control and PLL dynamics during MG transition, two transition scenarios are tested and the results of the proposed regulators are verified by comparing them with the reported method in [18] and the case without smooth regulators (W/O).

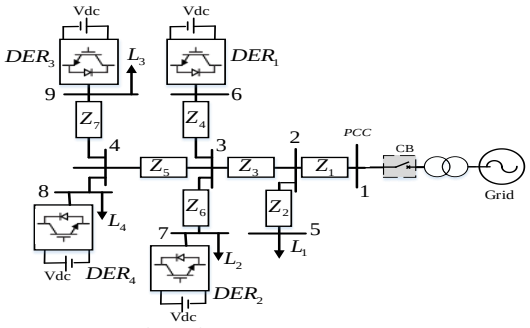

Fig. 6. Network model of MG for simulation study [18].

TABLE I
Electrical and Control Parameters of Simulation Case [18]

Parameters	Symbol	Value
DC Voltage	V_{dc}	650V
MG nominal voltage	V_{PCC}	325 V
Line 1 - impedance	Z_1	(0.0198+j0.0581) Ω
Line 2 - impedance	Z_2	(0.1107+j0.0028) Ω
Line 3 - impedance	Z3	(0.0198+j0.0581) Ω
Line 4 - impedance	Z_4	(0.0404+j0.0024) Ω
Line 5 - impedance	Z_5	(0.0768+j0.0113) Ω
Line 6 - impedance	Z_6	(0.0099+j0.0029) Ω
Line 7 - impedance	Z_7	(0.0513+j0.0054) Ω
Load 1	L_1	(5+j2) kVA
Load 2	L_2	(50+j27) kVA
Load 3	L_3	(20+j10) kVA
Load 4	L_4	(22+j11) kVA

A. Islanding transition scenario

In this scenario, the MG initially is in the GC mode and the DERs operate in 33% of their nominal power with unity power factor. At *t=3 s*, the MG is disconnected and goes to the islanding mode. The DERs detect the islanding mode through a passive islanding detection algorithm and change their operation mode into the grid-forming strategy. Fig. 7 and Fig. 8 show the active and reactive power of DERs during islanding transition. In Fig. 7, a peak value of 10% overshoot with prolonged oscillation can be observed in DER1 and DER2 without smooth regulators. With the proposed method of [18], the overshoot is dropped to 5%. The maximum overshoot percentage of the DERs' active power was reduced to below 1.2% by the proposed GCISSR, with a smooth behavior. Similarly, the reactive power of DER1 and DER3 experienced 54% and 27% overshoot with significant oscillations without regulators. These values are decreased to 22% and 13% according to the method in [18] and 10% and 7% by the proposed GCISSR. The PCC voltage and the MG frequency are depicted in Fig. 9.

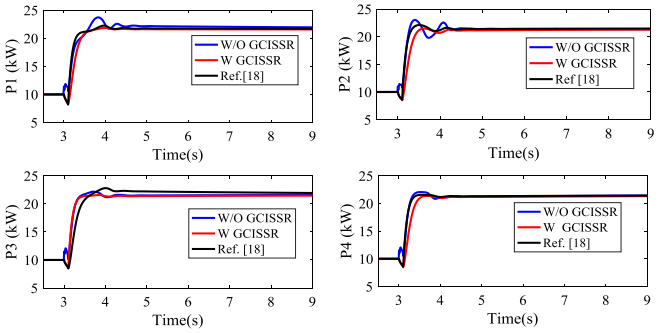

Fig. 7. DERs active power during islanding transition.

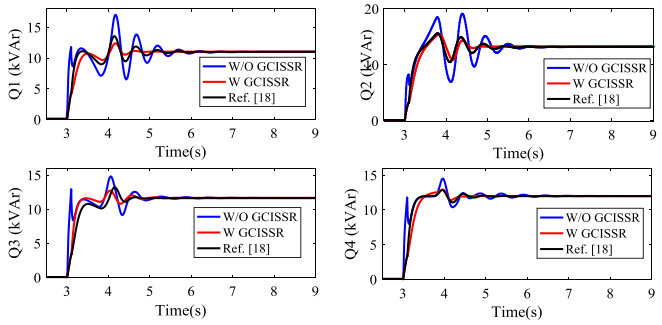

Fig. 8. DERs reactive power during islanding transition.

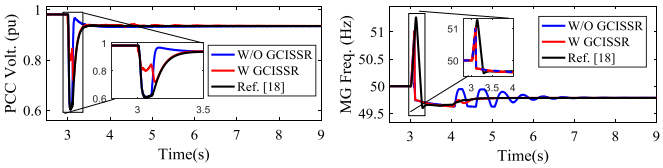

Fig. 9. PCC voltage and MG frequency during islanding transition.

The PCC voltage is decreased to 0.6 pu, 0.62 pu and 0.75 pu according to without regulator, regulator of [18] and proposed GCISSR, respectively. The MG frequency has oscillation behavior without regulators. With the method of [18], frequency is raised to 51.5 Hz after confirming islanding detection, while frequency has a small settling time with a smooth response.

B. Microgrid Reconnection transition scenario

At *t=25 s* the MG is reconnected to the main grid. Fig. 10 and Fig. 11 show the active and reactive power of DERs during reconnection transition. Without regulators, the active and reactive power of DERs have experienced a significant peak. While, with the proposed GCISSR, it can be seen that the active power of DERs track their references smoothly. The effect of PLL dynamics on the transition process can be deduced from differences in reactive power response between method of [18] and the proposed ISGCSR.

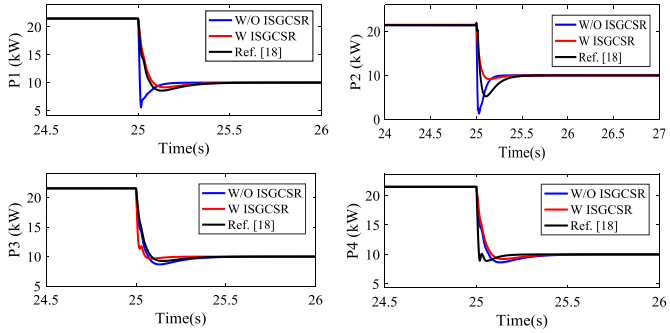

Fig. 10. DERs active power during reconnection of MG to grid.

This article has been accepted for publication in a future issue of this journal, but has not been fully edited. Content may change prior to final publication. Citation information: DOI 10.1109/TSG.2021.3094419, IEEE Transactions on Smart Grid

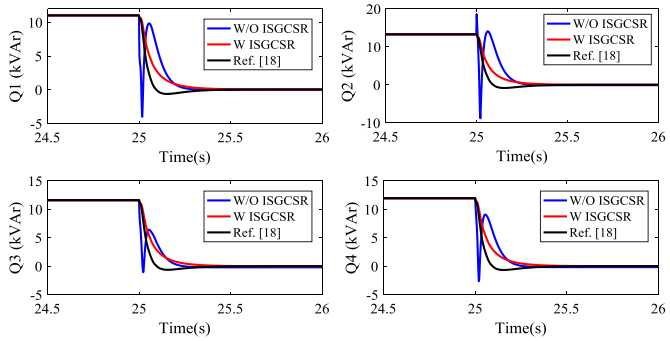

Fig. 11. DERs reactive power during reconnection of MG to grid.

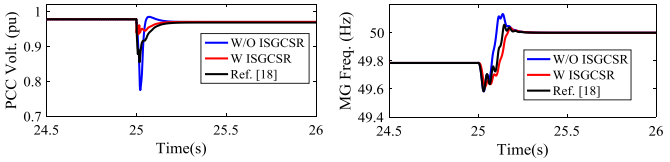

Fig. 12. PCC voltage and MG frequency during reconnection of MG to grid.

With the ISGCSR, the reactive power has no peak with a smooth response compared with the method of [18]. Fig. 12 shows the PCC voltage and the MG frequency during reconnection transition. After reconnection, the PCC voltage dropped to 0.77 pu. Using the method in [18], the PCC voltage is decreased to 0.85 pu, while it is settled to steady-state without any peak using the proposed ISGCSR.

C. Performance analysis

Opposed to the [18], in our proposed approach the effect of PLL dynamic during reconnection transition considered by adding (39), (40) and (43) in the IS to GC smooth regulator (ISGCSR) designing procedure. Actually, this item reflects the phase trajectory and its deviation in regulator design procedure. By a similar argument, inner control loops dynamics is considered during transition to islanding. Phase plane analysis is one of the most effective techniques for studying the behavior of systems while providing motion trajectories corresponding to initial condition. This analysis gives a very good insight of system behavior. So, the phase plane analysis is used to show the behavior of the proposed strategy during transition. Two dimensional phase plane based on *x1-x3* (P-Q) trajectory of DER2 is depicted in Fig. 13 for three different strategies during transition. Although, these three strategies converge to a stable equilibrium point, the proposed strategy provides the superior trajectory. Also, to evaluate the performance of the proposed controller, different simulation studies are performed and compared with the proposed strategy of [18] and with the case without smooth regulator. Comparison results are introduced in Table II and Table III respectively.

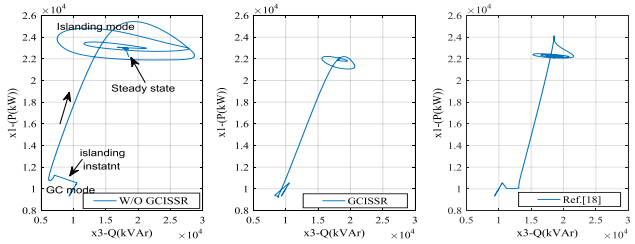

(a) (b) (c)

Fig. 13. State trajectory of the DER2 during transition from grid-connected to the islanding mode, (a) Without GCISSR, (b) With GCISSR, and (c) Ref. [18].

TABLE II
SIMULATION RESULTS COMPARISON BASED ON AVERAGE OF THE DERS' ACTIVE POWER

	Islanding transition		Reconnection transition	
	Overshoot (%)	Settling time (s)	Undershoot (%)	Settling time (s)
Without smooth regulator	10	1.49	39	0.5
Ref. [18]	4	1.3	12	0.3
The proposed strategy	1	1.15	7	0.2

TABLE III
SIMULATION RESULTS COMPARISON BASED ON AVERAGE OF THE DERS' REACTIVE POWER

	Islanding transition		Reconnection transition	
	Overshoot (%)	Settling time (s)	Undershoot (%)	Settling time (s)
Without smooth regulator	35	2.6	300	0.3
Ref. [18]	17	2	65	0.28
The proposed strategy	9	1.4	0	0.27

Although the proposed strategy mitigate transient response overshoots, its performance is not studied within MG with voltage sensitive load. To manage this issue using the proposed strategy, the modified voltage control loop with virtual impedance can be a proper choice.

D. Robustness analysis

The islanding detection algorithm is one of the effective factors in the microgrid transition. Generally, the imperfection of an islanding detection algorithm can be modeled by a trigger signal. According to [29], the maximum clearing time of protective devices for an interconnected system is suggested up to 300*ms*. To analyze the robustness of the proposed strategy, a simulation study is done with different islanding detection time duration. Fig. 14 shows the active power of DER2 during islanding transition with two clearing time of 150*ms* and 300*ms*. It can be found that the overshoot values regarding all three control strategies are amplified by increasing the islanding detection time. By comparing the strategies, the proposed strategy has the lowest overshoot values. It can be deduced that the active power of DER2 in the proposed method reaches the steady-state with a negligible transient for the maximum clearing time.

A similar study is done to demonstrate the performance of three control strategies against the premature reconnection process. It means that the closing command is sent to the circuit breaker (CB) before satisfying the IEEE.std.1547 synchronizing criteria [29]. Thus, it may make a significant transient in DERs' output. To investigate the performance of three control strategies against imperfect reconnection process, a simulation study is done with two different times where CB is closed at *t= 21s* and *t=25s*. Fig. 15 shows the active power of DER2 during reconnecting transition.

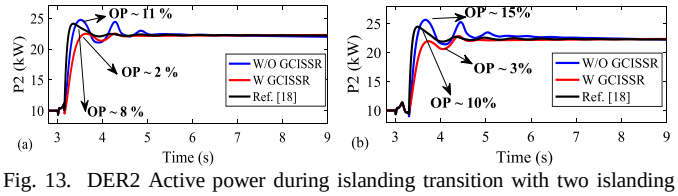

Fig. 13. DER2 Active power during islanding transition with two islanding detection time, (a) 150*ms* and (b) 300*ms*.

This article has been accepted for publication in a future issue of this journal, but has not been fully edited. Content may change prior to final publication. Citation information: DOI 10.1109/TSG.2021.3094419, IEEE Transactions on Smart Grid

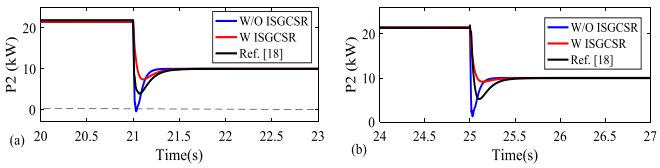

Fig. 14. Active power of DER2 during reconnecting transition with two CB closing time, (a) *t=21s* and (b) *t=25s*.

A noticeable transient can be easily found for three control strategies when CB is closed earlier. However, the proposed control strategy has a superior performance where DERs are suffered severe transient with two other control strategies.

V. Experimental Validation

To validate the feasibility of the proposed controller implementation, an inverter-based MG, shown in Fig. 16(a), is prototyped. A photo of the experimental setup is illustrated in Fig. 16(b). The hardware part of the MG is composed of two 2.2 kW Danfoss inverters in parallel, LCL filters, measurement sensors and a RL load. There is also a CB to connect/disconnect the MG to/from the grid. The inverters are supplied by a stiff DC voltage source. They can be operated in both GC and IS modes with grid-feeding and grid-forming strategies, respectively. The electrical and control parameters are given in Table IV. Meanwhile, the real time simulation platform (dSPACE 1006) and I/O boards are software parts of the MG. The control platform based on the proposed approach is simulated in MATLAB/Simulink environment. Then, the control platform is built in dSPACE using MATLAB compiler. The performance of the proposed regulators is investigated through two different scenarios including transition from GC to IS mode and vice-versa. The experimental results for the aforementioned studies are plotted in MATLAB using captured data from dSPACE Control Desk and represented in following.

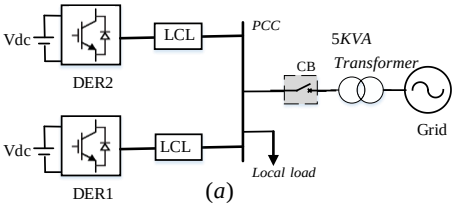

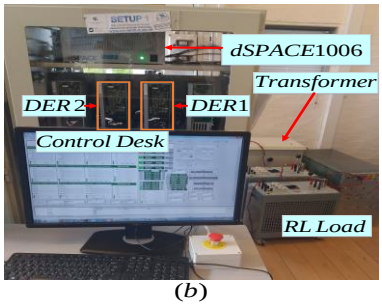

Fig. 15. Microgrid test system configuration: (a) electrical schematic, and (b) experimental setup.

TABLE IV
Electrical and Control Parameters of Experimental Test System

Parameters	Symbol	Value
DC Voltage	V_{DC}	650V
MG nominal voltage	V_g	325 V
Capacitance of LCL filter	C_f	25 μF
Inductances of LCL filter	L_f , L_c	1.8 mH
Nominal frequency	f	50 Hz
Switching frequency	f_s	10 kHz
Impedance of Loads	Z_{L1}	115+ j47.1
P-W droop coefficient	m	0.0064 rad/w.s
Q-V droop coefficient	n	0.02 V/VAr
LPFs cut-of frequency	w_c, w_m	2π rad/s, 200 rad/s
PI gains of PLL	k_p^θ, k_i^θ	0.1, 1
PI gains of voltage loop	k_p^v, k_i^v	0.25, 50
PI gains of current loop	k_p^c, k_i^c	0.35, 100

A. Transition from GC to IS Mode

Initially, the MG is connected to the main grid and DERs are operated in the grid-feeding strategy. The set-points for DERs are P^*=300W and Q^*=0 VAr where the power factor was set to unity. Due to an unintentional islanding at *t=3s*, CB opens thereby separating the MG. The parallel DERs share active and reactive power demanded from the local load, where each DER supply an average active and reactive power output of 540W and 220 VAr, respectively.

Fig. 17 and Fig. 18 provides the output voltage waveform and magnitude at PCC during islanding transition. The PCC voltage magnitude increases to 360 V without regulator (W/O), while it is limited to 328 V with GCISSR (W). The output currents of DER 1 and DER 2 during transition are depicted in Fig. 19 and Fig. 20, respectively. Moreover, the supplying output active and reactive power of DERs can be observed in Fig. 21 and Fig. 22, respectively. It can be found that the deviation in current and voltage has led to active power experience a noticeable overshoot ~16% of its steady-state value, see Fig. 21(a) and Fig. 22(a). On the contrary, the GCISSR decreases the overshoot impressively (2% of its steady-state value), which verifies the effectiveness of the proposed regulator in providing a smooth transition from GC to IS mode (see Fig. 21 (b) and Fig. 22(b)).

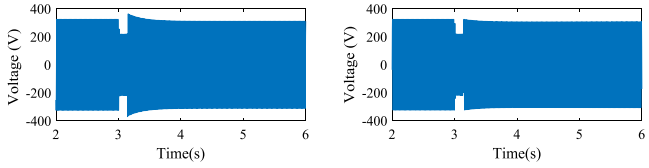

Fig. 16. PCC voltage waveform during transition from GC to IS mode: (a) without GCISSR, and (b) with GCISSR.

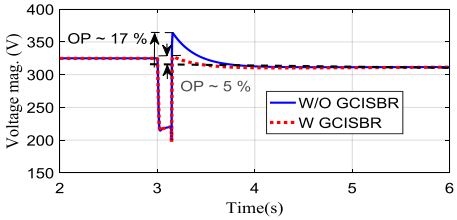

Fig. 17. PCC voltage magnitude during transition from GC to IS mode.

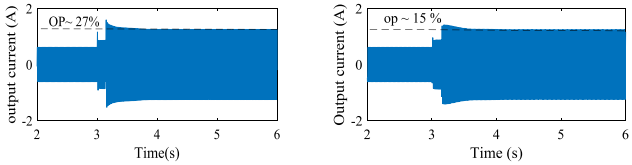

Fig. 18. Output current waveform during transition from GC to IS mode without smooth regulator: (a) DER 1, and (b) DER 2.

This article has been accepted for publication in a future issue of this journal, but has not been fully edited. Content may change prior to final publication. Citation information: DOI 10.1109/TSG.2021.3094419, IEEE Transactions on Smart Grid

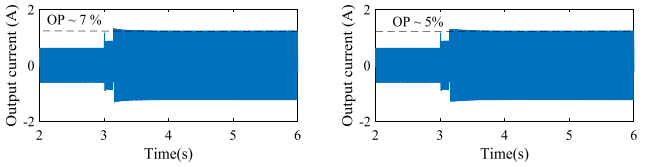

(a) (b)

Fig. 20. Output current waveform during transition from GC to IS mode with smooth regulator: (a) DER 1, and (b) DER 2.

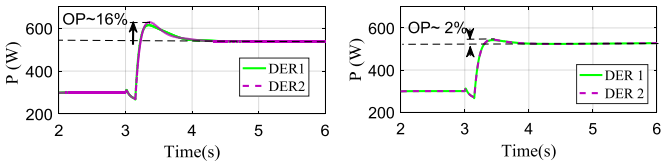

(a) (b)

Fig. 21. Active power of DERs during transition from GC to IS mode: (a) without GCISSR, and (b) with GCISSR.

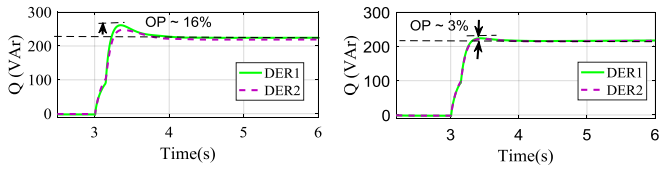

(a) (b)

Fig. 22. Reactive power of DERs during transition from GC to IS mode: (a) without GCISSR, and (b) with GCISSR.

B. Transition from IS to GC Mode

In this scenario, the effectiveness of the proposed ISGCSR is verified during the reconnecting transition of the MG to the main grid. The synchronization process with the main grid is done before the reconnection process. After issuing the resynchronizing command, the CB is closed at *t=15s*; thus, the DERs operation mode is changed from grid-forming to grid-feeding strategy. The set-points of the grid-feeding strategy of DERs are *P**=900W with unity power factor.

It can be seen from Fig. 23 and Fig. 24 that the voltage at PCC experiences an overshoot of 5V (~330V), while the PCC voltage raises up to 327V with ISGCSR regulator.

The output currents of DER 1 and DER 2 during MG reconnection are depicted in Fig. 25 and Fig. 26, respectively. The active power of DERs have a similar shape, which are shown in Fig. 27, for both cases of without (W/O) ISGCSR and with (W) ISGCSR. Without ISGCSR, the reactive power is suffered a 50% overshoot and raised to 358 VAr (see Fig. 28(a)). According to Fig. 28(b), the reactive power of DERs are mitigated to 259 VAr using ISGCSR.

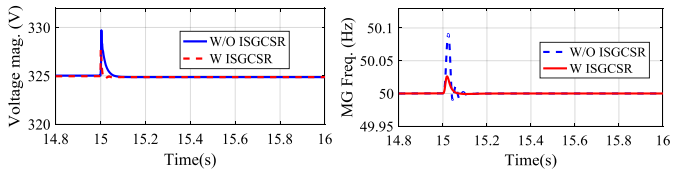

Fig. 23. PCC voltage and freq. during transition from IS to GC mode at *t=15s*.

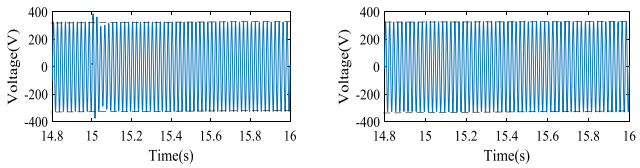

(a) (b)

Fig. 24. PCC voltage waveform during transition from IS to GC mode: (a) without GCISSR, and (b) with GCISSR.

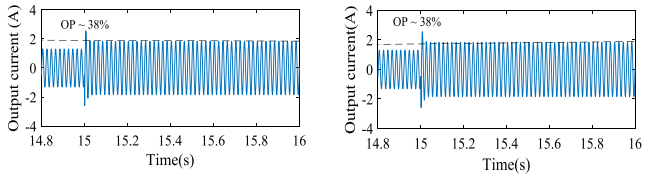

(a) (b)

Fig. 25. Output current waveform during transition from IS to GC mode without smooth regulator: (a) DER 1, and (b) DER 2.

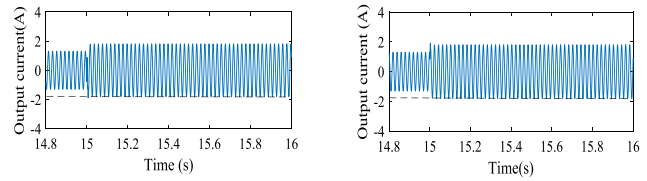

(a) (b)

Fig. 26. Output current waveform during transition from IS to GC mode with smooth regulator: (a) DER 1, and (b) DER 2.

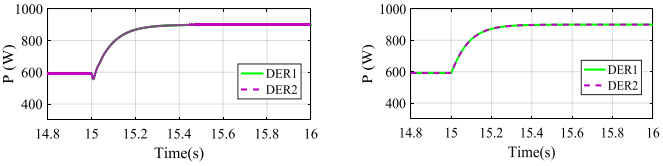

(a) (b)

Fig. 27. Active power of DERs during transition from GC to IS mode: (a) without ISGCSR, and (b) with ISGCSR.

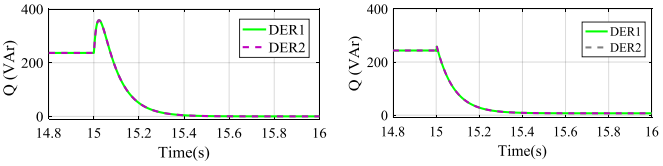

(a) (b)

Fig. 28. Reactive power of DERs during transition from GC to IS mode: (a) without ISGCSR, and (b) with ISGCSR.

VI. Conclusion

This paper proposes a control strategy with two smooth regulators based on a linear quadratic approach to guarantee a smooth transition between the AC microgrid operation modes. To design the proposed regulators, not only the droop mechanism but also the inner control loops and the PLL dynamics are taken into account. For each operation mode, an individual regulator is developed to minimize transients at DER output variables during transition process. The output of the regulators is a scalar constant state feedback which has a simple form and easy to implement. Experimental results verify the effectiveness of the proposed approach in mitigating overshoots in the voltage, current, and output power of DERs.

VII. Appendix

Appendix A: State Space Matrices of Grid-Forming Strategy

$$A=\begin{bmatrix} -w_c & 0 & 0 & 0 & 0 & 0 & 0 \\ -m & 0 & 0 & 0 & 0 & 0 & 0 \\ 0 & 0 & -w_c & 0 & 0 & 0 & 0 \\ 0 & 0 & -n & 0 & 0 & 0 & 0 \\ 0 & 0 & 0 & 0 & 0 & 0 & 0 \\ 0 & 0 & -k_p^v n & k_i^v & 0 & 0 & 0 \\ 0 & 0 & 0 & 0 & k_i^v & 0 & 0 \end{bmatrix} \quad B_1=\begin{bmatrix} -w_c & 0 & 0 & 0 & 0 \\ 0 & 1 & 0 & 0 & 0 \\ 0 & 0 & -w_c & 0 & 0 \\ 0 & 0 & 0 & 1 & 0 \\ 0 & 0 & 0 & 0 & 1 \\ 0 & 0 & 0 & k_p^v & 0 \\ 0 & 0 & 0 & 0 & k_p^v \end{bmatrix} \quad D_1=\begin{bmatrix} 0 & 0 & 0 & 0 & 0 \\ 0 & 0 & 0 & k_p^v k_p^c & 0 \\ 0 & 0 & 0 & 0 & k_p^v k_p^c \end{bmatrix}$$

$$B_2=\begin{bmatrix} w_c & 0 & 0 & 0 & 0 & 0\\ 0 & 0 & 0 & 0 & 0 & 0\\ 0 & w_c & 0 & 0 & 0 & 0\\ 0 & 0 & -1 & 0 & 0 & 0\\ 0 & 0 & 0 & -1 & 0 & 0\\ 0 & 0 & -k_p^v & 0 & -1 & 0\\ 0 & 0 & 0 & -k_p^v & 0 & -1 \end{bmatrix}$$

$$C=\begin{bmatrix} 0 & 1 & 0 & 0 & 0 & 0 & 0\\ 0 & 0 & -k_p^v k_p^c n & k_i^v k_p^c & 0 & k_i^c & 0\\ 0 & 0 & 0 & 0 & k_i^v k_p^c & 0 & k_i^c \end{bmatrix}$$

$$D_2=\begin{bmatrix} 0 & 0 & 0 & 0 & 0 & 0\\ 0 & 0 & 1-k_p^v k_p^c & 0 & -k_p^c & -L_f w_0\\ 0 & 0 & 0 & 1-k_p^v k_p^c & L_f w_0 & -k_p^c \end{bmatrix}$$

APPENDIX B: STATE SPACE MATRICES OF GRID-FEEDING STRATEGY

$$A=\begin{bmatrix} -w_m & 0 & 0 & 0 & 0 & 0 & 0\\ 1 & 0 & 0 & 0 & 0 & 0 & 0\\ k_p^\theta & k_i^\theta & 0 & 0 & 0 & 0 & 0\\ 0 & 0 & 0 & -w_m & 0 & 0 & 0\\ 0 & 0 & 0 & 1 & 0 & 0 & 0\\ 0 & 0 & 0 & 0 & 0 & -w_m & 0\\ 0 & 0 & 0 & 0 & 0 & 1 & 0 \end{bmatrix}$$

$$B_1=\begin{bmatrix} w_m & 0 & 0 & 0\\ 0 & 0 & 0 & 0\\ 0 & 1 & 0 & 0\\ 0 & 0 & w_m & 0\\ 0 & 0 & 0 & 0\\ 0 & 0 & 0 & w_m\\ 0 & 0 & 0 & 0 \end{bmatrix}$$

$$D_2=\begin{bmatrix} 0 & 1 & 0\\ 0 & 0 & 1\\ 0 & 0 & L_f w_0\\ 0 & -L_f w_0 & 0 \end{bmatrix}^T$$

$$D_1=0$$

$$B_2=\begin{bmatrix} -w_m & 0 & 0 & 0 & 0 & 0 & 0\\ 0 & 0 & 0 & -w_m & 0 & 0 & 0\\ 0 & 0 & 0 & 0 & 0 & -w_m & 0 \end{bmatrix}^T$$

$$C=\begin{bmatrix} 0 & 0 & 1 & 0 & 0 & 0 & 0\\ 0 & 0 & 0 & k_p^C & k_i^C & 0 & 0\\ 0 & 0 & 0 & 0 & 0 & k_p^C & k_i^C \end{bmatrix}$$

APPENDIX C: STATE FEEDBACK MATRICES

$$SF_{VCM}=\begin{bmatrix} 0 & -0.3 & 0 & 346.3 & 755.5 & 174.1 & 432.7 & 0 & 0 & 0.2 & 1.4 & 0.5 & -1.7 & 0.3 & -0.8 & -1.9 & 1 & -0.9 & 0 & 0.6 & 0.5\\ 0 & -0.9 & 0 & 169.9 & 382.6 & 87.2 & 218.2 & 0 & 0 & 0.4 & 1 & 0.3 & -0.9 & 0.9 & -0.4 & -1 & 0 & 0 & 0 & 0 & 0\\ 0 & 1.4 & 0 & -89.6 & -194.7 & -44.4 & -111.3 & 0 & 0 & -0.5 & -0.9 & -0.1 & 0.4 & -1.4 & 0.2 & 0.5 & 0 & 1.3 & 1 & 0.3 & 0.4\\ 0 & -0.9 & 0 & -160.3 & -202.8 & -55.9 & -127.6 & 0 & 0 & 0.8 & -0.6 & 0 & 0.5 & 0.9 & 0.2 & 0.6 & 0 & 0 & 0 & 0 & 0\\ 0 & 0 & 0 & -198.9 & -582.7 & -125.4 & -322.4 & 0 & 0 & -0.5 & -0.4 & -0.5 & 1.3 & 0 & 0.5 & 1.4 & 0 & 0 & 0 & 0 & 0 \end{bmatrix}$$

$$SF_{CCM}=\begin{bmatrix} -2.5 & -97.5 & 8.5 & 13.3 & 3544.5 & 9.9 & 3019 & 12 & 12.2 & 7.4 & -6 & -8.5 & -12 & -10.2 & -0.9 & -0.3 & -1.6 & -0.8\\ 120.2 & 5416 & 511 & 186.5 & 8618.3 & 102.1 & 5800 & 29.2 & -36.4 & -82.8 & -66 & -511 & -29.2 & -19.7 & 56 & 16.6 & 93.9 & 49.5\\ 15.5 & -705.2 & -76.7 & -29.5 & -1738.4 & -12.1 & -435 & -5.9 & 5.4 & 11.7 & 9.4 & 76.7 & 5.9 & 1.5 & -6.9 & -2 & -11.5 & -6.1\\ 9.8 & 445 & 45.8 & 6.6 & -2331 & -7.4 & -3701 & -7.9 & -16.9 & -14.3 & 1.6 & -45.8 & 7.9 & 12.5 & 4.3 & 1.3 & 7.3 & 3.8 \end{bmatrix}$$

VIII. REFERENCES

[1] A. Bidram, A. Davoudi, F. L. Lewis, and S. S. Ge, "Distributed adaptive voltage control of inverter-based microgrids," *IEEE Trans. Energy Conver.*, vol. 29, no. 4, pp. 862-872, Dec. 2014.

[2] J. M. Rey, M. Castilla, J. Miret, A. Camacho, and R. Guzman, "Adaptive slope voltage control for distributed generation inverters with improved transient performance," *IEEE Tran. Energy Conver.*, vol. 34, no. 3, pp. 1644-1654, Sept. 2019.

[3] S. M. Ashabani, and Y. A.-r. I. Mohamed, "New family of microgrid control and management strategies in smart distribution grids—analysis, comparison and testing," *IEEE Trans. Power Syst.*, vol. 29, no. 5, pp. 2257-2269, Sept. 2014.

[4] H. Han, X. Hou, J. Yang, J. Wu, M. Su, and J. M. Guerrero, "Review of power sharing control strategies for islanding operation of AC microgrids," *IEEE Trans. Smart Grid*, vol. 7, no. 1, pp. 200-215, Jan. 2016.

[5] D. E. Olivares, A. Mehrizi-Sani, A. H. Etemadi, C. A. Cañizares, R. Iravani, M. Kazerani, A. H. Hajimiragha, O. Gomis-Bellmunt, M. Saeedifard, and R. Palma-Behnke, "Trends in microgrid control," *IEEE Trans. Smart Grid*, vol. 5, no. 4, pp. 1905-1919, Jul. 2014.

[6] M. B. Delghavi, and A. Yazdani, "Sliding-mode control of ac voltages and currents of dispatchable distributed energy resources in master-slave-organized inverter-based microgrids," *IEEE Trans. Smart Grid*, vol. 10, no. 1, pp. 980-991, Jan. 2019.

[7] S. M. Ashabani, and Y. A.-R. I. Mohamed, "A flexible control strategy for grid-connected and islanded microgrids with enhanced stability using nonlinear microgrid stabilizer," *IEEE Trans. Smart Grid*, vol. 3, no. 3, pp. 1291-1301, Sept. 2012.

[8] S. Sajadian, and R. Ahmadi, "Model predictive control of dual-mode operations z-source inverter: islanded and grid-connected," *IEEE Trans. Power Electron.*, vol. 33, no. 5, pp. 4488-4497, May 2018.

[9] P. C. Sekhar, and R. R. Tupakula, "Model predictive controller for single-phase distributed generator with seamless transition between grid and off-grid modes," *IET Gener. Transm. Distrib.*, vol. 13, no. 10, pp. 1829-1837, Jun. 2019.

[10] A. Micallef, M. Apap, C. Spiteri-Staines, and J. M. Guerrero, "Single-phase microgrid with seamless transition capabilities between modes of operation," *IEEE Trans. Smart Grid*, vol. 6, no. 6, pp. 2736-2745, Nov. 2015.

[11] X. Shu, F. Wang, L. Ren, X. Feng, and G. Xu, "Control strategy ensuring multi-mode seamless transition for a single-phase LCL inverter." *43rd Annual Conference of the IEEE Industrial Electronics Society*, Beijing, China pp. 995-1000, Oct/Nov. 2017.

[12] G. Lou, W. Gu, J. Wang, J. Wang, and B. Gu, "A unified control scheme based on a disturbance observer for seamless transition operation of inverter-interfaced distributed generation," *IEEE Trans. Smart Grid*, vol. 9, no. 5, pp. 5444-5454, Sept. 2018.

[13] T. H. Nguyen, K. Al Hosani, N. Al Sayari, and A. R. Beig, "Seamless transition scheme between grid-tied and stand-alone modes of distributed generation inverters," *3rd International Future Energy Electronics Conference and ECCE Asia*, Kaohsiung, Taiwan, pp. 344-349, Jun. 2017.

[14] B. Singh, G. Pathak, and B. K. Panigrahi, "Seamless transfer of renewable-based microgrid between utility grid and diesel generator," *IEEE Trans. Power Electron.*, vol. 33, no. 10, pp. 8427-8437, Oct. 2018.

[15] G. G. Talapur, H. Suryawanshi, L. Xu, and A. Shitole, "A reliable micro-grid with seamless transition between grid connected and islanded mode for residential community with enhanced power quality," *IEEE Trans. Ind. Appl.*, vol. 54, no. 5, pp. 5246-5255, Sept/Oct. 2018.

[16] C. Wang, B. Liang, and J. He, "An enhanced power regulation and seamless operation mode transfer control through cooperative dual-interfacing converters," *IEEE Trans. Smart Grid*, vol. 9, no. 6, pp. 5576-5587, Nov. 2018.

[17] Z. Liu, and J. Liu, "Indirect current control based seamless transfer of three-phase inverter in distributed generation," *IEEE Trans. Power Electron*, vol. 29, no. 7, pp. 3368-3383, Jul. 2014.

[18] D. Das, G. Gurrala, and U. J. Shenoy, "Linear quadratic regulator-based bumpless transfer in microgrids," *IEEE Trans. Smart Grid*, vol. 9, no. 1, pp. 416-425, Jan. 2018.

[19] S. Fekri, M. Athans, and A. Pascoal, "Robust multiple model adaptive control (RMMAC): A case study," International Journal of Adaptive Control and Signal Processing, vol. 21, no. 1, pp. 1-30, Feb. 2007.

[20] N. Sadati, M. Hosseinzadeh, and G. A. Dumont, "Multi-model robust control of depth of hypnosis," Biomedical Signal Processing and Control, vol. 40, pp. 443-453, Feb. 2018.

[21] M. Ganjian-Aboukheili, M. Shahabi, Q. Shafiee, and J. M. Guerrero, "Seamless transition of microgrids operation from grid-connected to islanded mode," *IEEE Trans. Smart Grid*, vol. 11, no. 3, pp. 2106 - 2114, May 2020.

[22] S. Yazdani, M. Ferdowsi, and P. Shamsi, "Internal model based smooth transition of a three-phase inverter between islanded and grid-connected modes," *IEEE Trans. Energy Conver.*, vol. 35, no. 1, pp. 405-415, Mar. 2020.

[23] J. Kim, J. M. Guerrero, P. Rodriguez, R. Teodorescu, and K. Nam, "Mode adaptive droop control with virtual output impedances for an inverter-based flexible AC microgrid," *IEEE Trans. Power Electron.*, vol. 26, no. 3, pp. 689-701, Mar. 2011.

[24] C.-L. Chen, Y. Wang, J.-S. Lai, Y.-S. Lee, and D. Martin, "Design of parallel inverters for smooth mode transfer microgrid applications," *IEEE Trans. Power Electron.*, vol. 25, no. 1, pp. 6-15, Jan. 2010.

[25] Y. Du, H. Tu, and S. Lukic, "Distributed control strategy to achieve synchronized operation of an islanded MG," *IEEE Trans. Smart Grid*, vol. 10, no. 4, pp. 448-4496, Jul. 2018.

[26] X. Hou, Y. Sun, J. Lu, X. Zhang, L. H. Koh, M. Su, and J. M. Guerrero, "Distributed hierarchical control of AC microgrid operating in grid-connected, islanded and their transition modes," *IEEE Access*, vol. 6, pp. 77388-77401, Nov. 2018.

[27] M. C. Turner, and D. J. Walker, "Linear quadratic bumpless transfer," *Automatica*, vol. 36, no. 8, pp. 1089-1101, Aug. 2000.

[28] J. C. Vasquez, J. M. Guerrero, M. Savaghebi, J. Eloy-Garcia, and R. Teodorescu, "Modeling, analysis, and design of stationary-reference-frame droop-controlled parallel three-phase voltage source inverters," *IEEE Trans. Ind. Electron.*, vol. 60, no. 4, pp. 1271-1280, Apr. 2013.

[29] *IEEE Standard for Interconnecting Distributed Resources With Electric Power Systems*, IEEE standard 1547, 2003.